

Efficiently serving large multimedia models using EPD Disaggregation

Gursimran Singh* Xinglu Wang† Ivan Hu* Timothy Yu* Linzi Xing* Wei Jiang‡
Zhefeng Wang‡ Xiaolong Bai‡ Yi Li‡ Ying Xiong* Yong Zhang* Zhenan Fan*

*Huawei Technologies Canada, †Simon Fraser University, ‡Huawei Cloud

Abstract

Large Multimodal Models (LMMs) extend Large Language Models (LLMs) by handling diverse inputs such as images, audio, and video, but at the cost of adding a multimodal encoding stage that increases both computational and memory overhead. This step helps convert raw inputs into tokenized representations that inflate the token sequence for the prefill phase, negatively impacting key Service Level Objectives (SLOs) like time to first token (TTFT) and end-to-end throughput. We introduce Encode-Prefill-Decode (EPD) Disaggregation, a novel framework that separates the encoding, prefill, and decode stages onto dedicated resources. Unlike current systems, which bundle encoding and prefill together, our disaggregation approach alleviates memory bottlenecks, mitigates synchronization delays, and supports flexible batching. Specifically, we employ a new caching mechanism for multimodal tokens, enabling asynchronous transfer of multimodal tokens and introduce an integrated module to find optimal config for EPD system and minimize resource usage while maximizing SLO-based performance metric. Experimental evaluations with popular LMMs show substantial gains in memory efficiency (up to 15× lesser for encoding-stage GPUs), that supports upto 22× higher batch sizes, 10× more number of images/request, 2.2× higher kv cache size. Further, it leads to significant improvements in end-to-end throughput (up to 57% better), and latency metrics (TTFT up to 71% lower), compared to systems that do not disaggregate. Our findings underscore the potential of EPD disaggregation to enable resource-efficient and high-performance multimodal inference at scale.

1. Introduction

Large Language Models (LLMs) have revolutionized language understanding and reasoning, achieving superhuman performance across a variety of tasks [1, 4]. Recently, the scope of these models has expanded to include multiple modalities, such as images, audio, and videos, result-

ing in the advent of Large Multimodal Models (LMMs) [5, 11, 21]. LMMs enable users to interact with diverse data types, such as posing questions about visual scenes or analyzing audio clips, thereby unlocking novel applications across fields like healthcare, autonomous systems, and creative industries.

However, serving LMMs in an efficient manner presents unique challenges. Meeting strict Service Level Objectives (SLOs) such as end-to-end throughput (E2ETP), time to first token (TTFT), and time per output token (TPOT) becomes increasingly difficult given the additional computational and memory demands introduced by processing multimodal data [12]. Unlike LLMs, where inference involves prefill and decoding stages, LMMs require an additional encoding stage to process raw multimodal inputs (e.g., images or videos) into tokenized representations. This stage is computationally intensive, especially for high-resolution or complex multimodal inputs, and often produces a substantial number of additional tokens [20]. The resulting increase in tokens inflates resource consumption and leads to quadratic growth in prefill-stage compute demands, adversely impacting SLO attainment.

Disaggregating the prefill stage from the decode stage has emerged as a well-studied solution in the literature to improve inference efficiency for LLMs [7, 9, 14, 15, 24]. By assigning separate resources to each stage, prefill-decode disaggregation enables independent optimization of batching, scheduling, and resource allocation strategies, significantly enhancing system throughput and memory utilization. However, these techniques fail to address the challenges of LMM deployment, where the addition of an encoding stage fundamentally alters the resource dynamics. The encoding stage, with its high computational and memory overhead, introduces token inflation and dependency bottlenecks that ripple across subsequent stages, necessitating a rethinking of disaggregation strategies to accommodate multimodal workloads.

In current systems, the encoding and prefill stages are typically aggregated into a single monolithic and synchronous step executed on the same set of GPUs. This

approach assumes that combining encoding and prefill can simplify implementation, but in practice, it exacerbates inefficiencies such as memory bottlenecks, limited batching flexibility, and synchronization delays. Specifically, simultaneous loading of both the multimodal encoder and LLM onto the same GPUs restricts memory for higher-resolution inputs or larger batch sizes, while the sequential execution of encoding and prefill introduces delays for encoding-light requests that must wait for encoding-heavy ones in the same batch. As a result, such aggregation leads to suboptimal resource utilization and poor SLO performance, making it clear that current solutions are inadequate for LMM workloads.

To address these challenges, we propose Encode-Prefill-Decode (EPD) Disaggregation, a framework that decouples the encoding, prefill, and decode stages, assigning each with dedicated resources to operate independently. This disaggregation enables customized batching, parallelization, and scheduling strategies for each stage, optimizing resource utilization while reducing contention. By separating the multimodal encoder from the LLM on distinct GPUs, the system significantly improves memory efficiency, allowing for larger batch sizes and higher-resolution inputs. Additionally, asynchronous token transfer between stages minimizes latency, ensuring smooth and efficient processing. As a result, EPD disaggregation achieves better memory utilization, higher throughput, and improved compliance with critical SLOs like TTFT, TPOT, and E2ETP.

The major contributions of this work are as follows:

- We identify major challenges and performance bottlenecks due to which the performance of existing multimodal inference systems is suboptimal. Specifically, these stem from encoding and prefill being a single monolithic and synchronous step that results in poor performance owing to inefficient utilization of memory and computation resources.
- We propose an efficient system for LMM inference that relies on the novel idea of disaggregating encoding and prefill stages. Our approach addresses key challenges of resource allocation, inter-stage communication, and performance optimization within this framework. Specifically, we propose allocation of a new cache to store multimodal tokens on encoding and prefill stage that allows asynchronous transfer of multimedia tokens in an efficient manner.
- We formulate the search for the optimal configuration of the EPD disaggregated system as a black-box optimization problem. This approach is simple yet practical because, on the one hand, it allows for a flexible search space that easily incorporates realistic configurations, including various parallelization strategies, GPU allocation, batch size selection, and complex scheduling strategies. On the other hand, it is computationally efficient, as a

simulation outputs performance metrics (e.g., goodput or E2ETP) without actually deploying the system.

- We provide a detailed experimental analysis of our method with respect to baselines on various popular LMM models, namely MiniCPMv 2.6, InternVL2-8B, and InternVL2-26B. The results demonstrate the superiority of our method in terms various aspects, like memory (upto 15x lesser), facilitating upto 22x bigger batch sizes, 10x more number of images/ request, 2.2x higher kv cache size. Further, our method achieves significantly improved performance in terms of SLO attainment (upto 90-100% more), TTFT latency (upto 71% lesser), and E2ETP (upto 57% better).

2. Related Work

Serving LLMs and LMMs, which often consist of billions of parameters, poses significant challenges due to slow inference speeds [12, 25]. Efficiently serving these models to billions of users while adhering to stringent Quality of Service (QoS) criteria has therefore become an active area of research [6]. This has led to the development of numerous production-grade systems, such as vLLM [10], TorchServe [17], NVIDIA Triton [13], SGLang [23], and HuggingFace Text Generation Inference (TGI) [18], that integrate ideas emerging from recent advancements in this field.

Throughput-Optimized Inference Systems: One prominent direction of research focuses on improving throughput, a critical system-level metric, by optimizing GPU utilization. For instance, Orca [22] proposed continuous batching, a technique that dynamically increases batch size without interrupting ongoing decoding, thereby enhancing GPU efficiency. vLLM [10] introduced paged KV cache management, which reduces memory fragmentation and frees up GPU memory, enabling larger batch sizes and ultimately boosting throughput. Similarly, SARATHI [2] introduced chunked prefill, which splits prefill requests into smaller chunks and piggybacks decoding requests alongside them to improve GPU utilization. However, these systems are designed for LLMs and do not account for the resource-intensive multimodal encoding step unique to LMMs, which precedes the prefill phase.

Latency-Optimized Inference Systems: Another line of work focuses on improving user-level metrics, such as request latency, for individual queries. For example, FastServe [19] employs iteration-level preemptive scheduling to reduce latency caused by head-of-line blocking in throughput-optimized systems. To gain finer control over TTFT and TPOT, approaches like SplitWise [14], DistServe [24], and DéjàVu [16] disaggregate the prefill and decode stages, mitigating interference between them. However, these methods are designed for LLMs and overlook the resource-intensive encoding step present in LMMs. Since encoding is coupled with prefill, these systems suffer from

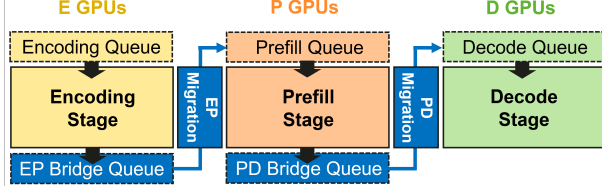


Figure 1. The inference pipeline of EPD Disaggregation system.

poor TTFT latency, particularly when the resolution and quantity of multimodal data are large.

We propose disaggregation of encoding from prefill, enabling fine-grained control over batching, scheduling, and parallelization strategies, thereby achieving better latency and throughput in LMMs.

3. Method

3.1. LMM System

At a high level, the LMM system transforms multimodal data and a text prompt into a coherent textual output. The system receives three types of input: (1) a *text prompt* i_p , which provides the context for the task (e.g., “What is the content of the image?”), (2) *multimodal data* i_m , which includes images, videos, or other sensory inputs (e.g., one or more images of a cat), and (3) *sampling data* i_s , which consists of parameters such as the desired number of output tokens and temperature settings. The system processes these inputs to generate a *text output* o , which is the model’s response (e.g., “The image contains a cat.”). For simplicity, we focus on the visual modality in this paper, but the framework is extensible to other types of multimodal data as well.

3.2. EPD Disaggregation

Disaggregating an LMM system involves breaking the inference process into distinct stages, each with specific inputs and outputs. As shown in Figure 1, the system follows a multi-stage inference pipeline consisting of three primary components: *encoding*, *prefill*, and *decode*. Additionally, the transitions between these stages are managed through *EP-migration* and *PD-migration*, which handle the transfer of data between encoding-prefill and prefill-decode stages, respectively. In the following, we describe each stage and the transformations involved.

Encoding (E): The multimodal input i_m is processed by the multimodal encoder (MME) E , which converts the input data into multimodal tokens v_t^e on encoding stage GPUs. These tokens represent a high-dimensional embedding of the input and serve as the foundation for the next stage of the pipeline.

$$v_t^e = E(i_m) \quad (1)$$

EP-migration: Once the encoding stage E completes processing, the generated multimodal tokens v_t^e must be transferred to the prefill stage P . This transfer is managed by the *EP-migration* function ψ_{EP} , which handles the migration of tokens from the encoding worker’s cache to the prefill worker’s cache.

$$v_t^p = \psi_{EP}(v_t^e) \quad (2)$$

Here, v_t^p represents the tokens in the prefill stage after migration.

Prefill (P): The multimodal tokens v_t^p arrive at the Prefill stage P , along with the text prompt i_p . In this stage, the system initializes the Key-Value (KV) cache kv_1^p and generates the first output token o_1^p . The KV cache stores context and intermediate states, which are necessary for the subsequent decoding stage.

$$kv_1^p, o_1^p = P(v_t^p, i_p) \quad (3)$$

PD-migration: After the prefill stage generates the initial token o_1^p and updates the KV cache to kv_1^p , the data must be transferred to the decode stage D . This transfer is managed by the *PD-migration* function ψ_{PD} , which ensures that the KV cache and the generated token are correctly handed off to the decode worker.

$$kv_1^d, o_1^d = \psi_{PD}(kv_1^p, o_1^p) \quad (4)$$

Decode (D): The Decode phase D operates iteratively, using the KV cache kv_t^d and the previously generated token o_t^d to generate the next token o_{t+1}^d and update the KV cache to kv_{t+1}^d . This autoregressive process continues until the desired output sequence is produced.

$$kv_{t+1}^d, o_{t+1}^d = D(kv_t^d, o_t^d) \quad (5)$$

Each token generation step depends on the previous token and the context stored in the KV cache, ensuring the system generates contextually accurate and coherent outputs.

3.3. System Design and Optimization

Figure 2 illustrates the architecture of our EPD Disaggregated Inference system. Each stage of the pipeline—Encoding, Prefill, and Decoding—features fully independent instances capable of running the corresponding stage. These instances are designed to operate in DP mode, meaning multiple instances per stage can process different requests concurrently, ensuring scalability and efficiency.

Each instance comprises a scheduler, responsible for scheduling requests, block managers (responsible for managing cache(s)), and multiple workers. The workers operate in tensor-parallel (TP) and/or pipeline-parallel (PP) mode, where each worker holds only a subset of the model weights and the corresponding caches required for the stage.

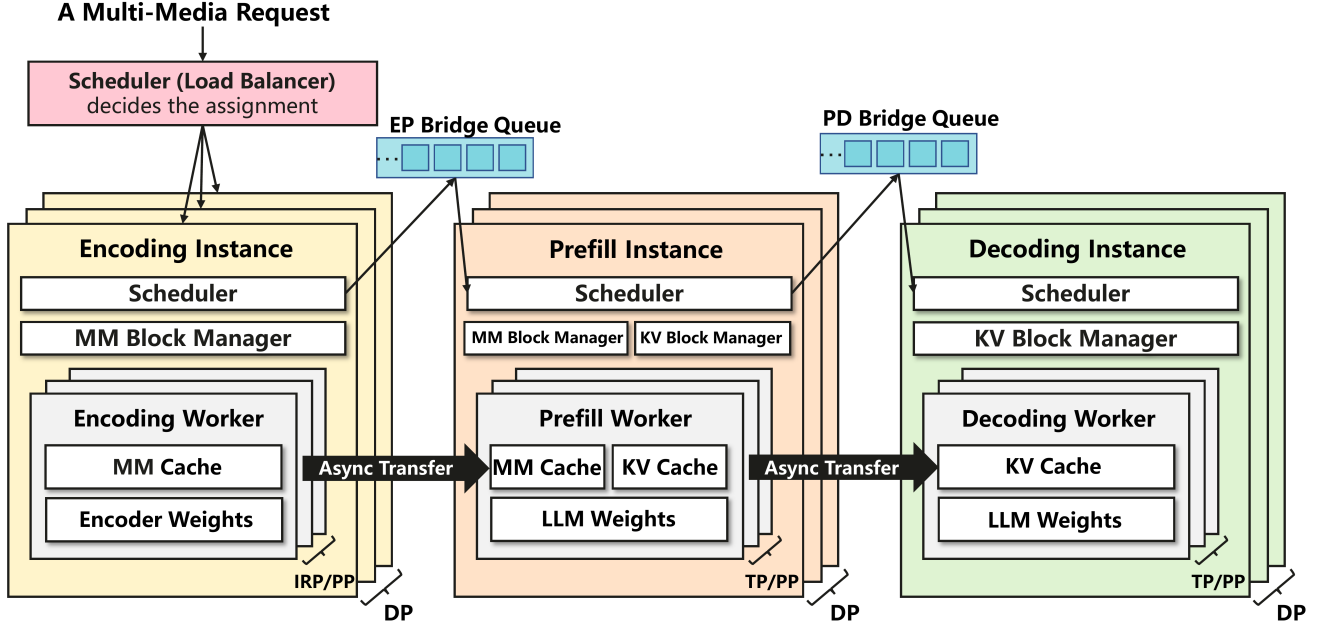


Figure 2. System architecture of the proposed EPD Disaggregated Inference. It consists of three stages. In each stage, data parallelism (DP) means multiple instances serve in parallel. Each instance encompasses pipeline-parallel (PP) workers and tensor-parallel (TP) workers. For the encoding stage, since intra-request parallel (IRP) is better than TP, we use IRP instead of TP workers. MM stands for Multi-Media.

In the Encoding Stage, instances/ workers only load the MME as the LLM is not required at this stage. Similarly, only the MM cache is necessary to be initialized. In the Prefill Stage, instances load the LLM to handle prefill operations, but the MME is no longer required. These instances utilize both the MM cache and the KV cache to efficiently manage multimedia and key-value data associated with the request. In the Decoding Stage, instances also load the LLM, focusing exclusively on decoding tasks. The MME is not required at this stage, and only the KV cache is utilized.

All cache transfers occur when an instance pulls a request from its respective queue, ensuring that data is moved only when necessary. Further, our system incorporates several techniques to optimize the performance of the disaggregated LMM pipeline, with a primary focus on reducing latency (Section 3.3.2), managing resources effectively (Section 3.3.3), and ensuring smooth token transfers between stages (Section 3.3.1).

3.3.1. Asynchronous Token Transfer

To minimize latency during token transfers between stages, our system supports direct, asynchronous token transfers via high-bandwidth NVLink/ InfiniBand / NVSwitch channels. The transfer occurs asynchronously, allowing the system to continue processing new requests while the token transfer is in progress. Specifically, we maintain a mul-

timodal cache (MM cache) on both encoding and prefill workers. When a request completes the encoding stage, its tokens are first stored in the encoding worker’s MM cache, freeing the encoding worker to serve subsequent requests immediately.

An independent asynchronous event loop continually monitors for completed encoding tasks. When a request’s tokens become available, this event loop initiates a direct transfer of the tokens to the prefill worker’s MM cache. Because the transfer is asynchronous, the system can process other tasks in parallel without stalling. Once the token transfer is confirmed, the corresponding MM cache entries at the encoding stage are cleared to reclaim memory for future requests.

To manage these cache regions efficiently, we introduce an MMBlockManager. For each incoming request, the MMBlockManager precomputes the number of cache blocks the request will require and allocates them accordingly. After the request transitions from the encoding to the prefill stage and the tokens are transferred, those blocks are reassigned or de-allocated, enabling flexible cache usage even under heavy workloads.

3.3.2. Intra-Request Parallel (IRP)

Often, multimodal requests include multiple high-resolution images, each of which is partitioned into patches for high-resolution encoding. For modern LMMs, the

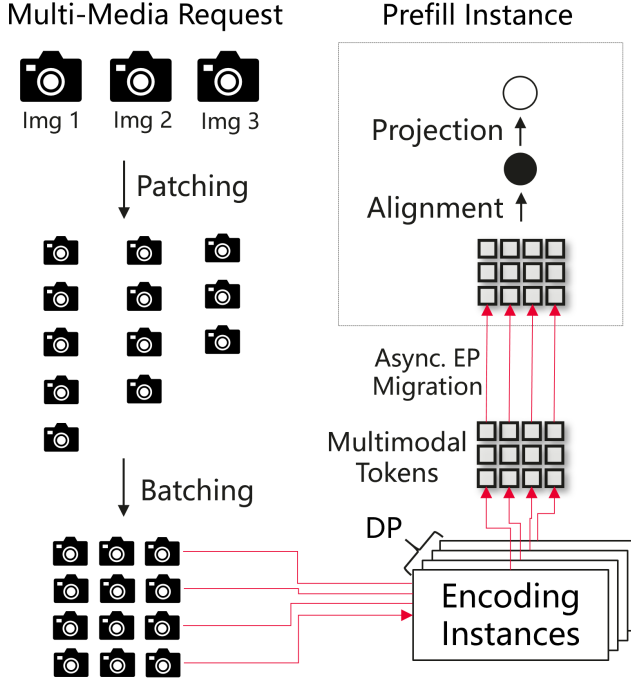


Figure 3. The illustration of Intra-Request Parallel.

encoder responsible for processing these patches can be large, making the encoding phase computation-bound. Hence, if a request is processed serially, the encoding phase can become a bottleneck, adding significant delay to the first token latency TTFT.

To address this, we introduce Intra-Request Parallel (IRP), which splits a single request’s image patches among multiple encoding workers operating in data-parallel mode. We are guided by the intuition that these patches are encoded independently and hence can be processed in a parallel and asynchronous manner. As depicted in Fig. 3, each encoding worker receives a distinct subset of patches, computes the corresponding token representations, and transfers them to the prefill stage independently and asynchronously. This means that patches assigned to one encoding worker can finish and begin transferring without waiting for patches processed by other workers.

Once all the patch-level tokens arrive at the prefill stage, they are aligned, projected, and merged to form the complete set of multimodal tokens for the request. The request then proceeds through the prefill stage as usual, with the corresponding LLM processing the aggregated multimodal and prompt tokens. By allowing concurrent encoding of patches across multiple workers, IRP effectively reduces end-to-end latency and improves the utilization of available encoding resources, especially for high-resolution inputs with large numbers of patches.

3.3.3. Optimized Resource Allocation

The system dynamically determines configurations such as batch sizes, scheduling strategies, and parallelization approaches for each stage of the pipeline. This ensures that critical performance metrics are kept near optimal, based on the workload samples collected during deployment. These workload samples are gathered in real time from a recent time window. If the optimal performance metrics vary significantly in subsequent time windows, the system may adjust the configuration of the EPD pipeline accordingly.

We leverage a black-box optimization algorithm to select configurations, which minimizes GPU usage and maximizes a critical performance metric. For online serving scenarios, we define *goodput* as the key performance metric. Goodput represents the maximum request rate at which 90% of requests meet the TTFT and TPOT requirements. In offline scenarios, where TTFT and TPOT constraints are less critical, we use E2ETP as the performance metric. By the nature of performance metrics, the optimized config will minimize pipeline inefficiencies (e.g., idle time) and ensure allocated resources are utilized efficiently.

The optimization problem is formulated as:

$$\max_{(\mathbf{p}, \mathbf{b}, \mathbf{s}) \in \mathcal{X}} f(\mathbf{p}, \mathbf{b}, \mathbf{s}) - \beta \text{cost}(\mathbf{p}) \quad (6)$$

where \mathcal{X} is the search space for system configurations, including parallelization configs \mathbf{p} , max batch size configs \mathbf{b} , and scheduling configs \mathbf{s} . These variables are vectors, with each element representing the configuration of an individual instance. Here, an instance can handle requests independently, encompassing the (sub-)workers for tensor parallelism and pipeline parallelism. Since instances within a stage process different requests in parallel, we term it data parallelism. Note that $\mathbf{p}, \mathbf{b}, \mathbf{s}$ can have variable lengths, as the number of instances is itself a configurable parameter. For i -th instance, we denote its stage as $\text{Stage}_i \in \{E, P, D\}$.

- **Parallelization:** Let \mathbf{p} denote the vector of parallel configurations for all instances. For the i -th instance, if it is a prefill or decoding instance, then its configuration p_i includes: p_i^{TP} , the number of GPUs used for tensor parallelism; and p_i^{PP} , the number of GPUs used for pipeline parallelism. If it is an encoding instance, considering intra-request parallelism (IRP) does not require communication, which is better than TP, we only use IRP. Therefore, we overload the symbol $p_i^{\text{TP}} = p_i^{\text{IRP}}$ to denote the number of GPUs used for IRP. If the cost per GPU is a constant c , then the total cost is: $\text{cost}(\mathbf{p}) = c \sum_{p_i \in \mathbf{p}} (p_i^{\text{TP}} \times p_i^{\text{PP}})$.
- **Max Batch Size** determines how many requests are processed simultaneously during the encoding, prefill, and decoding stages. Let \mathbf{b} denote the batch size config for all instances. For i -th instance, b_i is its max batch size. This

config involves a trade-off between latency and throughput. Larger batch sizes improve throughput by enabling parallel processing but may increase latency if the stages become compute-bound.

- **Scheduling** involves two main questions: First, to which workers or queues should the requests be assigned? Second, how should the order of requests be determined within a queue? We adapt strategies from the DistServe framework [24]. In the encoding stage, when a request arrives, it is assigned and pushed to an instance queue. In the prefill and decode stages, a global queue is used, and each engine pulls from this queue when available. Possible assignment strategies in the encoding stage include Round-Robin or Least-Loaded First for assigning requests. Once a request is assigned to a worker’s queue, we can apply ordering strategies like first-come-first-serve or shortest-job-first, or more complex strategies that prioritize requests based on their Service Level Objectives (SLOs). For simplicity, we constrain that all instances within the same stage share the same scheduling strategy.

In the objective of the problem 6, β is a weight that controls the trade-off between performance and cost reduction. In a black-box setting, the performance function $f(\cdot)$ is unknown and must be evaluated through simulations to obtain the performance metric values. To solve the optimization problem, existing methods such as random search, evolutionary algorithm, Bayesian optimization [3], and parametric iterated local search [8] can be employed to find the optimal configuration. We adopt random search to find a near-optimal config for its simplicity.

4. Implementation

EPD is a fully capable distributed serving system for LMMs, comprising several key components: a load estimation module, a resource allocation module, a RESTful API frontend, and a multimodal-aware orchestration layer. The entire framework is implemented with a mix of Python and C++/ CUDA implementations, ensuring superior scalability and performance. To facilitate integration, we repurpose the distributed execution engine from vLLM, which supports numerous popular LLMs and LMMs, allowing easy adaptation of new models into our disaggregated framework with minimal effort.

The API interface adheres to OpenAI’s multimodal specifications, enabling users to specify parameters such as output length, temperature, and multimodal data inputs.

The scheduler is specifically designed for the disaggregated EPD framework, dynamically managing batch sizes and enabling asynchronous execution of the encoding, prefill, and decoding phases. The load estimation module ensures efficient GPU allocation across these phases, adapting to changing workload demands in real time.

Our repurposed distributed execution engine uses Ray actors to implement GPU workers, which manage multimodal and key-value caches, and coordinate the independent execution of the encoding, prefill, and decoding tasks. Furthermore, it supports 3D parallelism, incorporating Data Parallelism (DP), Tensor Parallelism (TP), and Pipeline Parallelism (PP) to maximize resource utilization and scalability.

The orchestration layer includes custom CUDA kernels optimized for parallelism in the encoding and prefill phases. These kernels enable efficient management of paged multimodal caches and ensure seamless asynchronous transfer of multimodal tokens between encoding and prefill GPUs. The orchestration layer oversees the execution of encoding, prefill, and decoding instances, handling tasks such as request distribution, KV cache transmission, and result aggregation. For efficient data movement, the system employs NCCL for inter-node GPU communication and asynchronous `CudaMemcpy` for intra-node transfers, ensuring smooth operations without disrupting GPU computations across the disaggregated EPD framework.

5. Experiments

In this section, we analyze and compare the performance of the proposed EPD disaggregation method against the baselines.

Baseline Methods: We compared our proposed method EPD against two popular baselines: DistServe [24] and vLLM [10]. The DistServe baseline implements the prefill-decode (PD) disaggregation approach, where the prefill and encoding are executed on one set of GPUs, while the decode phase is disaggregated on a separate GPUs. In contrast, the vLLM baseline adopts a monolithic architecture, where all three stages runs on the same set of GPUs. In addition, we also consider an ablation of our method EPD without the IRP feature, named as EPD-IRP.

Since DistServe was originally designed for LLMs, we extended its framework to support LMMs. This required extending the request handling infrastructure to process multimodal data, modifying the block manager to accommodate multimodal tokens, and changing the execution engine from SwiftTransformer to vLLM, which natively supports multiple LLMs. The change to vLLM also ensured consistency in execution engine across all baselines, eliminating potential confounding performance differences arising from variations due to the execution engine.

Models: We utilized three LMMs in our analysis: MiniCPM-V 2.6 [21], InternVL 2.0 8B, and InternVL 2.0 26B [5]. These models are renowned for their advanced capabilities in processing and understanding multimodal data.

MiniCPM-V 2.6 integrates a SigLip-400M vision encoder, comprising 400 million parameters, with a Qwen2-7B language model, containing 7.6 billion parameters, cul-

#I/R	MiniCPMv 2.6 8B		InternVL 8B		InternVL 26B	
	TTFT	TPOT	TTFT	TPOT	TTFT	TPOT
2	1.40	0.04	1.20	0.05	3.50	0.07
4	2.60	0.04	2.40	0.06	7.05	0.08
6	3.90	0.06	3.55	0.09	11.00	0.95
8	5.10	0.06	5.00	0.18	15.00	0.15

Table 1. Thresholds for TTFT and TPOT (in seconds) used for SLO computation across various models and number of images per request (#I/R) in the experiments.

minating in a total of 8 billion parameters. It excel in tasks involving single-image, multi-image, and video comprehension, even surpassing GPT-4V in these domains [21].

InternVL 2.0 8B features an InternViT-300M-448px vision encoder with 300 million parameters, paired with an internlm2_5-7b-chat language model comprising 7.7 billion parameters, totaling 8 billion parameters. Similarly, InternVL 2.0 26B combines an InternViT-6B-448px-V1-5 vision encoder with 6 billion parameters and an internlm2-chat-20b language model containing 20 billion parameters, resulting in 26 billion parameters. These configurations result in models with 8 billion and 26 billion parameters, respectively.

Datasets: To analyze its performance across diverse scenarios, we utilized custom synthetic workload for all experiments. This approach offered the flexibility to systematically vary parameters such as prompt length, number of images per request, image resolution, output length, and sampling settings. This controlled experimental setup allowed us to assess the system’s robustness and adaptability under different workload configurations, ensuring a comprehensive evaluation of its efficiency and scalability. The length of input tokens in the prompt (excluding multimodal tokens) was fixed to 22. The length of output tokens were fixed to 10 in end-to-end experiments and 1 in the first token generation experiments.

Evaluation Metrics: We evaluate the system based on runtime performance and memory consumption. The runtime performance is assessed using the TTFT and TPOT metrics for online settings, and E2ETP for offline settings. These metrics are defined as follows:

- **TTFT:** The time elapsed from the creation of a request in the Request Generator until the first token is received by the Decoder. This metric captures the responsiveness of the system to incoming requests.
- **TPOT:** The time elapsed from the arrival of the first token at the Decoder to the arrival of the last token at the Output Consumer, divided by the number of output tokens. This metric reflects the per-token latency for generating outputs.
- **E2ETP:** The end-to-end throughput of the system, measured in terms of requests completed per second. This

metric evaluates the system’s ability to handle high request volumes in offline settings.

- **SLO Attainment:** The percentage of requests that meet predefined Service Level Objectives (SLOs), such as TTFT and TPOT thresholds. This metric assesses the system’s ability to deliver consistent performance under operational constraints.
- **Goodput:** The rate of successfully completed requests that meet SLO criteria, measured in requests per second. This metric emphasizes the system’s effective processing capacity, excluding failed or non-compliant tasks.

For memory benchmarking experiments, we analyze the baselines by evaluating the benefits of available free memory. Additional free memory can facilitate higher batch sizes, accommodate more images per request, or enable larger key-value (KV) cache sizes. We demonstrate the advantages of our proposed approach using these memory-related metrics, highlighting its ability to enhance system scalability and performance.

Implementation Details We conducted our experiments using a cluster of 8 NVIDIA A100 GPUs (82GB), which provided the computational resources necessary for evaluating the proposed system. Each server was equipped with 128 CPUs and 1TB of RAM. The CUDA version was 12.2. Flash attention-2 was used for the attention implementation. We use FP16 precision for all experiments.

To ensure a fair comparison, we standardized key performance-affecting settings of the inference engine across all baselines. Specifically, these include a block size of 16; a maximum of 2048 blocks per request; context tokens capped at 49,152, and decoding tokens at 81,920 per batch. The scheduling policy for all stages was set to First-Come-First-Served (FCFS). Further, to allow enough resources for memory-heavy multimodal requests to execute, KV cache GPU utilization was set to 50%, and the maximum number of multimedia data of 32 was imposed per prompt. The size of multimodal cache was fixed to 3000 across all models, and the vLLM inference engine was run in eager mode. Finally, for the vLLM inference engine, we used the version 0.6.1.post1 that represents a stable version for multimodal inference.

In our online experiments, requests were sent to the inference engine using a Poisson arrival process with a fixed λ , representing the number of requests per second. Each trial was executed until 100 requests were completed, ensuring sufficient data for consistent performance analysis. Further, to optimize TTFT and TPOT in this latency-sensitive setting, we disabled batching by setting batch sizes to 1 for the encoding, prefill, and decoding stages.

5.1. SLO Attainment for End-to-End Generation

In this experiment, we evaluate the end-to-end SLO performance of the proposed method (EPD), an ablation of

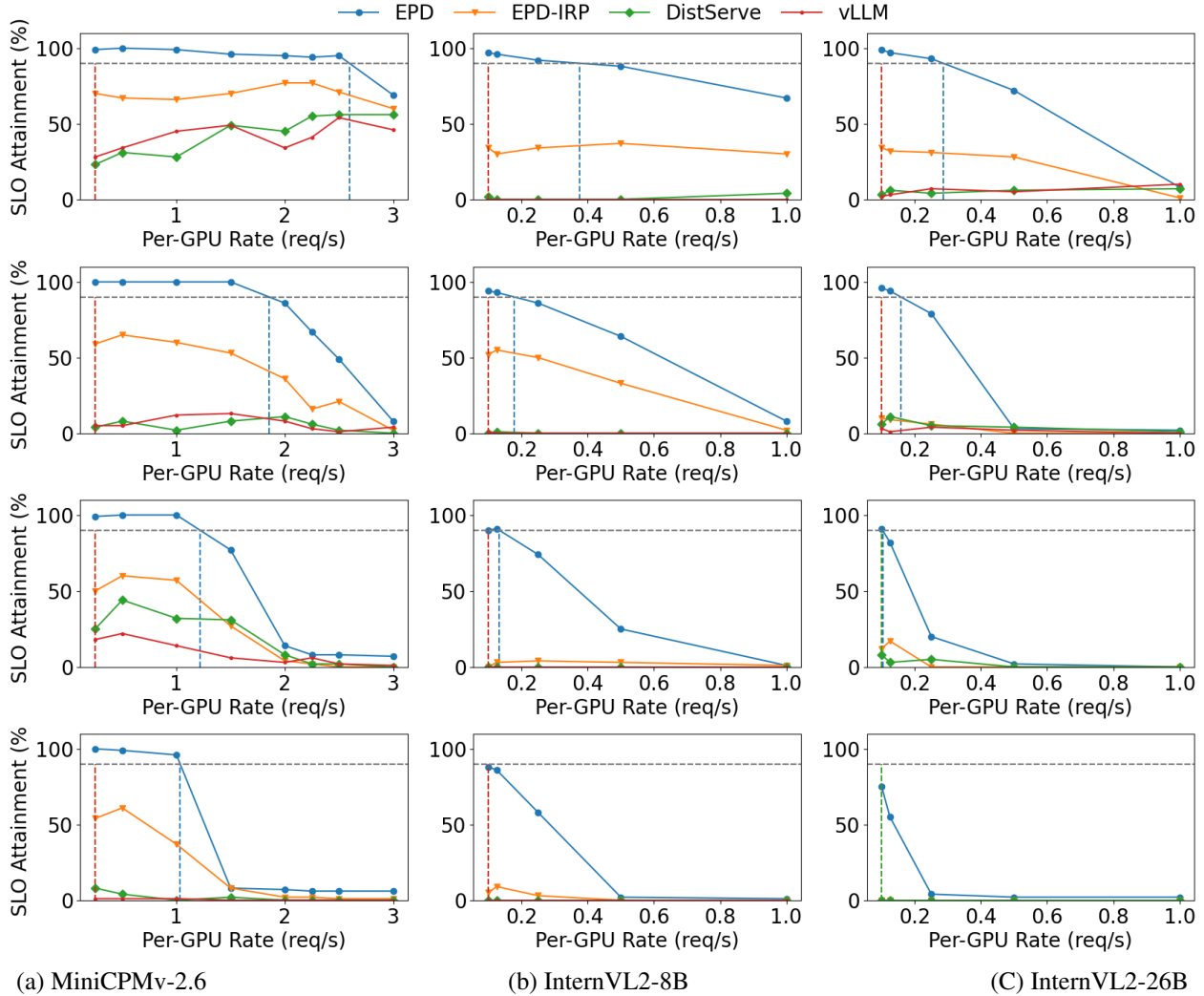


Figure 4. SLO attainment for end-to-end inference across various models and image counts per request. Column (a) presents results for the MiniCPMv 2.6 model with 2, 4, 6, and 8 images per request (from top to bottom). Column (b) and (c) show results for InternVL2-8B and InternVL2-26B, respectively. The image resolution is fixed at 4K. As observed, EPD significantly outperforms all baselines across all configurations. EPD-IRP means that IRP is *disabled* in EPD system.

our method without IRP (EPD-IRP) and existing state-of-the-art baselines, DistServe and vLLM. The setup involves 8 NVIDIA A100 GPUs serving 100 multimodal requests, arriving via a Poisson process with a fixed rate (λ) representing the number of requests per second. We tested three different models—MiniCPMv 2.6, InternVL2-8B, and InternVL2-26B—under varying image counts per request. All images were fixed at a 4K resolution of 4032x3024 pixels. The SLO criteria for each configuration, shown in Tab. 1, establish latency upper bounds for both TTFT and TPOT, ensuring timely token generation and consistent decoding performance.

The results for MiniCPMv 2.6 (left), InternVL2-8B (middle), and InternVL2-26B (right) are presented in Fig. 4. Each row corresponds to a different image count per re-

quest, specifically 2, 4, 6, and 8, listed from top to bottom. The X-axis represents the per-GPU request rate (requests per second, req/s), while the Y-axis shows the SLO attainment percentage, defined as the proportion of requests meeting both TTFT and TPOT thresholds. The black dotted line indicates the 90% SLO attainment threshold, and the corresponding request rate represents the goodput for 90% SLO attainment.

EPD-IRP demonstrates significantly higher SLO attainment compared to other baselines. At lower request rates, EPD-IRP achieves over 90% SLO attainment in most scenarios. This performance advantage is attributed to EPD-IRP’s ability to parallelize the computationally intensive image encoding step across multiple GPUs, mitigating the delay due to computationally-heavy encoding step. The

second-best performer, EPD, achieves an SLO attainment close to 50% in many cases. However, the prior work, DistServe and vLLM, perform the worst, often attaining SLO percentages below 10%. These baselines suffer from interference between encoding and prefill stages, resulting in consistently poor SLO attainment. On the other hand, EPD can mitigate this interference due to disaggregation of encoding and prefill, however it lacks the parallelization ability of EPD-IRP.

As the image count per request increases (from top to bottom rows), the SLO attainment for all baselines declines, particularly at higher request rates. This decline reflects the growing computational demands of processing multiple high-resolution images within a single request. In the most demanding scenario, with 16 images per request (bottom-most row), SLO attainment drops significantly for all baselines. However, EPD-IRP continues to maintain reasonable SLO attainment, especially at lower request rates, highlighting its robustness under heavy workloads.

Finally, as we move from left to right across the plots, the change in model leads to progressively worse performance for all baselines. The InternVL models are prefill-heavy, with prefill stages taking substantially longer due to the generation of a higher number of image tokens. As a result, TTFT suffers from additional queuing delays at the prefill stage, especially at higher request rates. This effect becomes more pronounced when transitioning from the 8B (middle) to the 26B (right) model. In contrast, the MiniCPMv (left) model is optimized to generate fewer image tokens, making it encoding-heavy rather than prefill-heavy. Consequently, it avoids the queuing delays observed in the InternVL models and exhibits better latency characteristics overall.

5.2. First Token Generation Latency

In this experiment, we analyze the TTFT performance of the proposed method (EPD), an ablation of our method without IRP (EPD-IRP) and an existing state-of-the-art baseline, DistServe. Unlike prior analyses that focused on end-to-end inference, this experiment isolates the prefill phase of the computation, as the generation of the first token represents a critical latency bottleneck due to large number of prefill tokens in multimodal workloads. Note that in this setup the DistServe baseline is equivalent to vLLM since the decoding phase is not involved.

Fig. 5 shows the results for the three models: MiniCPMv 2.6, InternVL2-8B, and InternVL2-26B, shown in the left, middle, and right plots, respectively. Each subplot presents box plots of TTFT distributions, with the x-axis representing the number of images per request and the y-axis showing the TTFT. The results are generated using 100 requests issued at a request rate of 0.25 for the MiniCPMv 2.6 and 0.08 for the InternVL2-8B and InternVL2-26B models. We

limit the number of images per request (x-axis) on the basis of the respective model’s capacity.

As shown in the figure, EPD-IRP significantly outperforms the two baselines, EPD and DistServe, across all three models. Specifically, the TTFT can be upto 71.9%, 32.8%, and 44.9% lower than the DistServe baseline for the MiniCPMv 2.6, InternVL2-8B, and InternVL2-26B models, respectively. This performance advantage stems from its intra-request parallelization, which enables the multimedia data within each request to be encoded in parallel, whereas the baselines process this data sequentially.

Notably, EPD also demonstrates a slight performance improvement over DistServe, highlighting the independent benefits of disaggregating the encoding and prefill stages, even without full parallelization. In this case, the TTFT can be upto 9.8%, 4.9%, and 1.0% lower for the MiniCPMv 2.6, InternVL2-8B, and InternVL2-26B models, respectively.

Further, we also observe that the margin of improvement becomes increasingly pronounced as the number of images per request grows. These results highlight the ability of EPD-IRP to efficiently handle the computational demands of multimodal workloads, especially as the number of input images and overall complexity increase.

5.3. Memory Savings through Stage Disaggregation

This section demonstrates the significant memory savings achieved by disaggregating the encoding and prefill stages in the EPD system. In existing systems, such as DistServe and vLLM, the encoding and prefill stages are co-located on the same GPUs, requiring each GPU to load both the MME and the LLM. This co-location results in higher memory consumption, as both models must be loaded simultaneously on the same GPUs.

In contrast, the proposed disaggregated system optimizes memory usage by assigning the encoding stage to GPUs that load only the MME, while the prefill stage is handled by separate GPUs that load only the LLM. This separation significantly reduces memory requirements for both stages.

The memory savings achieved through this disaggregation are substantial. Specifically, the encoding-stage GPUs experience memory reductions of approximately 95%, 96.2%, and 78.3% for the MiniCPMv 2.6, InternVL2-8B, and InternVL2-26B models, respectively. On the other hand, the prefill-stage GPUs achieve memory savings of about 5%, 3.7%, and 21.6% for the same models. In practice, the memory savings could be as high as 15x lower as encoding stage do not need to load the KV cache which is only required for prefill. These reductions in memory usage enable the EPD system to allocate resources more efficiently, allowing for the support of additional tasks and models, as demonstrated in the subsequent experiments.

EPD Supports a Higher Number of Images per Request: Tab. 2 compares the maximum number of images

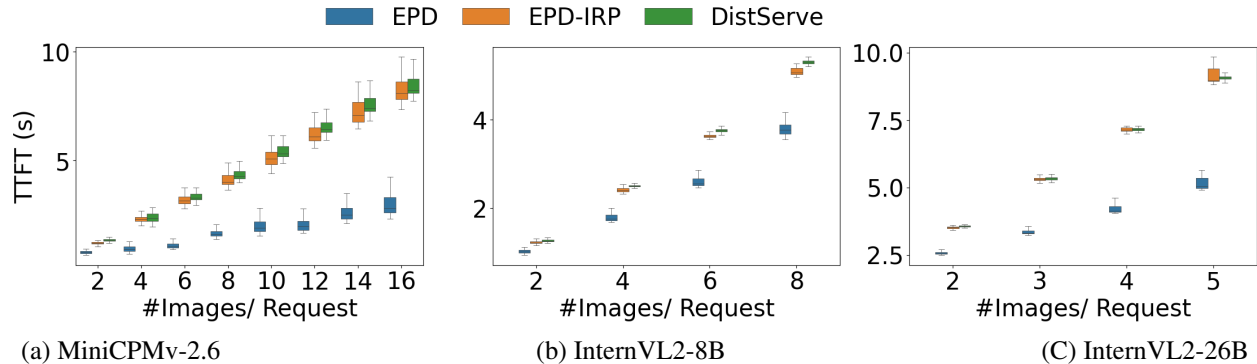


Figure 5. Distribution of TTFT (y-axis) for various #Images/ Request (x-axis) for the MiniCPMv 2.6 (left), InternVL2-8B (middle), and InternVL2-26B (right) models. Requests arrive following a Poisson distribution with a fixed request rate (λ). Note that, when comparing TTFT, vLLM is equivalent to DistServe, hence it is skipped. EPD-IRP means that IRP is disabled in EPD system.

per request supported by the disaggregated (EPD) and aggregated (DistServe or vLLM) systems across three multi-modal models: MiniCPMv, InternVL2-8B, and InternVL2-26B. The experiment was conducted at three different image resolutions, with a fixed batch size of 1 and 80% of the available memory allocated for KV cache.

For the MiniCPMv model, the EPD approach demonstrates a significant advantage in handling a higher number of images per request. At a resolution of 313x234, EPD supports up to 490 images per request, compared to just 77 for the aggregated DistServe system, resulting in a more than $6x$ improvement. At the 787x444 resolution, EPD can handle 165 images per request, which is a $6.3x$ increase over DistServe’s limit of 26. Even at the highest resolution (4032x3024), EPD supports 49 images per request, while DistServe is limited to only 7, demonstrating a $7x$ improvement.

For the InternVL2-26B model, the improvements are equally striking. EPD supports up to $10x$ more images per request at both the 313x234 and 4032x3024 resolutions, and approximately $4x$ more at the 787x444 resolution, compared to DistServe.

Interestingly, for the InternVL2-8B model, both EPD and DistServe support the same number of images per request across all resolutions (19). This is because the InternVL2-8B model uses a relatively simple MME that is not memory-intensive, and the limit of 19 images is constrained by the maximum context length of the LLM rather than memory usage of the MME.

EPD Supports Higher Batch Sizes for Encoding and Prefill:

Tab. 3 compares the maximum supported batch sizes for the encoding (E) and prefill (P) stages across three multi-modal models: MiniCPMv, InternVL2-8B, and InternVL2-26B, at three different image resolutions. The number of images per request is fixed at 10, and each model uses a

Model	Image Reso.	DistServe	EPD
MiniCPMv 2.6	313,234	77	<i>490</i>
	787,444	26	<i>165</i>
	4032,3024	7	<i>49</i>
InternVL2-8B	313,234	19	19
	787,444	19	19
	4032,3024	19	19
InternVL2-26B	313,234	1	<i>10</i>
	787,444	11	<i>45</i>
	4032,3024	1	<i>10</i>

Table 2. Comparison of maximum supported number of images/request. Batch size is fixed to 1. KV cache is allocated as 80% of the available free memory. Experiment done on A800 GPU with 82GB memory. Higher (*italicized*) is better.

different patching strategy, leading to varying numbers of image patches. The last three columns show the maximum batch size that can be supported for each configuration without encountering out-of-memory (OOM) errors. For the EPD approach, batch sizes for encoding and prefill are listed separately, as these processes run independently on separate GPUs. In contrast, for the DistServe baseline, encoding and prefill share the same batch size since both stages are executed sequentially on a single GPU.

The EPD approach significantly outperforms the DistServe baseline in terms of supported batch sizes. For instance, with the InternVL2-26B model at a resolution of 787x444, EPD supports a batch size of 22 for encoding, while the DistServe baseline can only handle a batch size of 1, representing a $22x$ improvement. On the other hand, with the MiniCPMv2.6 model at a resolution of 787x444, EPD supports a batch size of 29 vs 2 for the DistServe baseline, representing a $14.5x$ improvement for prefill.

EPD Supports Larger KV Cache Sizes: Tab. 4 com-

Model	Image Reso.	#Patch	DistServe	EPD	
			E, P	E	P
MiniCPMv 2.6	313,234	1	7	<i>49</i>	<i>86</i>
	787,444	3	2	<i>16</i>	<i>29</i>
	4032,3024	10	OOM	4	9
InternVL2-8B	313,234	13	2	<i>15</i>	<i>2</i>
	787,444	3	9	<i>67</i>	<i>10</i>
	4032,3024	13	2	<i>15</i>	<i>2</i>
InternVL2-26B	313,234	13	OOM	6	<i>1</i>
	787,444	3	1	22	4
	4032, 3024	13	OOM	6	<i>1</i>

Table 3. Comparison of maximum supported E and P batch size. As seen, E, P batch sizes is much higher in EPD system in comparison to DistServe. Number of images/ request is fixed to 10. KV cache is allocated as 80% of the available free memory. Experiment done on one A800 GPU with 82GB memory. Higher (*italicized*) is better.

compares the maximum KV cache size that can be allocated in the disaggregated (EPD) system with that of the aggregated (DistServe or vLLM) system. In this experiment, the batch size is fixed at 1, and the image resolution is set to 4032×3024. We evaluate two LMM models, InternVL and MiniCPMv, with varying numbers of images per request.

The results clearly demonstrate that EPD supports significantly larger KV cache sizes than DistServe. For instance, for the InternVL2-26B model at 10 images per request, EPD can support a KV cache size of 80% vs 36% for Distserve, representing a *2.2x improvement*.

Notably, in certain scenarios—such as with the InternVL2-26B model and 20 images per request—the DistServe system encounters an Out of Memory (OOM) error, indicating that it cannot process 20 images even with a KV cache size of 0. Additionally, some configurations encounter an Out of Context Limit (OOCL) error, where the large number of encoding tokens generated by high image counts exceeds the LLM’s context limit during the prefill stage.

5.4. Throughput in Offline Settings

In this section, we demonstrate the benefits of the EPD method in terms of throughput, specifically focusing on its memory efficiency and the ability to support higher batch sizes for both the encoding (E) and prefill (P) stages.

Consider an offline scenario where a batch of requests is submitted, allowing the system to process them overnight with a focus on maximizing end-to-end (E2E) throughput. In the traditional DistServe method, memory is allocated for both the encoding and prefill stages on the same worker, which is constrained by the total memory capacity of the GPU.

This memory limitation becomes especially significant

Model	# Images/Req.	DistServe	EPD
MiniCPMv 2.6	5	86%	<i>99%</i>
	10	74%	<i>97%</i>
	20	49%	<i>95%</i>
	40	OOM	<i>92%</i>
	80	OOM	<i>OOCL</i>
InternVL2-8B	5	94%	<i>95%</i>
	10	89%	<i>91%</i>
	20	OOCL	<i>OOCL</i>
InternVL2-26B	5	67%	<i>89%</i>
	10	36%	<i>80%</i>
	20	OOM	<i>63%</i>
	40	OOM	<i>OOCL</i>

Table 4. Comparison of maximum supported KV cache size (in terms of percentage of free memory) on prefill node for various #images/ request. Image resolution fixed to 4K. OOM refers to Out of Memory and OOCL refers to Out of Context Limit. Experiments are done on A800 GPU with 82GB memory. Higher (*italicized*) is better.

in heterogeneous environments with low-end GPUs that have limited memory. In these cases, the DistServe method struggles to fully utilize low-end GPUs, as the combined memory demands of the encoding and prefill stages exceed the available memory. In contrast, our disaggregated EPD method is more cost-effective, as it assigns the low-end GPUs exclusively to the encoding stage, allowing better utilization of available memory.

In this experiment, we consider a less extreme scenario where the memory demands of the prefill workers in the DistServe method do not exceed the memory capacity of the low-end GPUs, allowing for a batch size of 1 for both the encoding and prefill stages.

We use 8 A800 GPUs for this experiment. For EPD, we allocate 5 GPUs for encoding (E), 2 GPUs for prefill (P), and 1 GPU for decoding (D), with the maximum batch sizes set to 8, 8, and 128 for E, P, and D, respectively. In the DistServe method, we allocate 7 GPUs for prefill (P) and 1 GPU for decoding (D), with the maximum batch sizes of 1 and 128, respectively. The workload consists of 1,000 requests, each with a single image, a simple prompt (“What is the content of this image?”), and a maximum of 10 output tokens.

We tune the system’s hyperparameters as outlined in Sec. 3.3.3 and evaluate their impact on throughput. The results are presented in Fig. 6.

The left plot illustrates the importance of selecting an appropriate GPU configuration. As described in Sec. 3.3.3, our algorithm automatically identifies that a 5E2P configuration (5 encoder and 2 prefill workers) maximizes E2E throughput.

The middle plot shows that EPD achieves superior

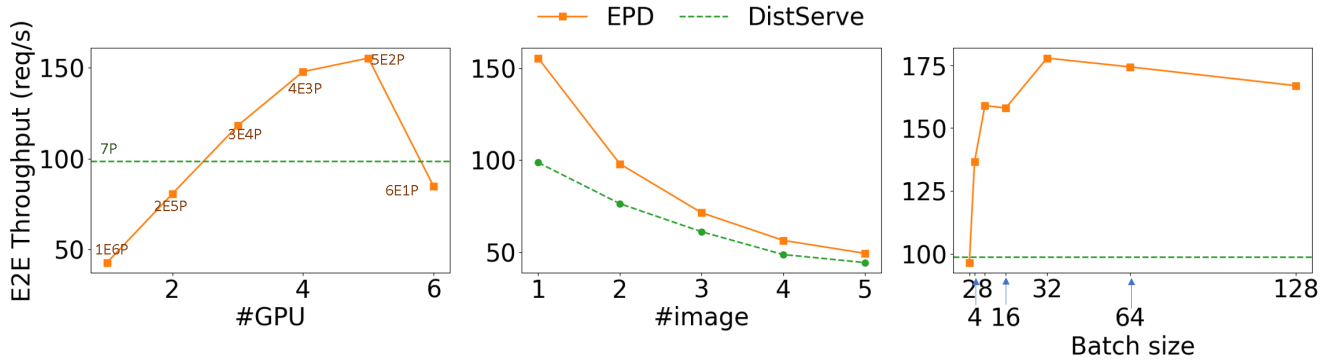


Figure 6. **Left:** The impact of tuning the number of encoding workers in the EPD method. The annotation ‘xEyP’ indicates that x encoders and y prefill workers are allocated for EPD, and ‘7P’ means that the DistServe always allocates 7 P workers for the encoding and prefill stage requests. **Middle:** The impact of the number of images per request in the workload. **Right:** The impact of encoding and prefill batch sizes in the EPD method (encoding and prefill batch sizes are set to be equal).

throughput when the number of images per request is low, demonstrating that EPD’s architecture prevents the encoder from becoming a compute-bound bottleneck.

The right plot highlights that EPD’s performance is relatively insensitive to encoding and decoding batch sizes, consistently outperforming the DistServe method. This flexibility allows us to either choose a relatively large batch size or rely on the algorithm in Sec. 3.3.3 to automatically select an optimal batch size.

6. Conclusion

In this paper, we present a novel approach to optimizing Large Multimodal Model (LMM) systems through the disaggregation of key processing stages. By separating the encoding, prefill, and decoding tasks into distinct stages, our system offers enhanced flexibility in resource allocation, enabling more efficient management of computational and memory resources. This disaggregation, combined with dynamic resource allocation, asynchronous token transfer, and advanced parallelization strategies, directly addresses several critical challenges in LMM deployment, including latency reduction, memory optimization, and efficient computational resource usage.

Our results demonstrate significant improvements in both throughput and memory efficiency, particularly in heterogeneous environments where resources are limited. By efficiently parallelizing the encoding and prefill stages, we are able to mitigate common bottlenecks and improve the scalability of multimodal inference tasks. Furthermore, the optimized memory management strategies ensure that the system can scale to handle larger models and more complex multimodal inputs, which are increasingly common in real-world applications.

The approach presented in this work represents a significant step forward in the development of scalable and effi-

cient systems for multimodal AI, offering a foundation for future research and practical applications in areas such as natural language processing, computer vision, and cross-modal understanding. In summary, our system provides a robust solution for improving the performance of LMMs, making them more efficient and adaptable for deployment in real-world, resource-constrained environments.

References

- [1] Josh Achiam, Steven Adler, Sandhini Agarwal, Lama Ahmad, Ilge Akkaya, Florencia Leoni Aleman, Diogo Almeida, Janko Altschmidt, Sam Altman, Shyamal Anadkat, et al. Gpt-4 technical report. [arXiv:2303.08774](https://arxiv.org/abs/2303.08774), 2023. 1
- [2] Amey Agrawal, Ashish Panwar, Jayashree Mohan, Nipun Kwatra, Bhargav S. Gulavani, and Ramachandran Ramjee. Sarathi: Efficient llm inference by piggybacking decodes with chunked prefills. [arXiv:2308.16369](https://arxiv.org/abs/2308.16369), 2023. 2
- [3] Borja Calvo, Ofer M Shir, Josu Ceberio, Carola Doerr, Hao Wang, Thomas Bäck, and Jose A Lozano. Bayesian performance analysis for black-box optimization benchmarking. In *Proceedings of the Genetic and Evolutionary Computation Conference Companion*, pages 1789–1797, 2019. 6
- [4] Yupeng Chang, Xu Wang, Jindong Wang, Yuan Wu, Linyi Yang, Kaijie Zhu, Hao Chen, Xiaoyuan Yi, Cunxiang Wang, Yidong Wang, et al. A survey on evaluation of large language models. *ACM Transactions on Intelligent Systems and Technology*, 15(3):1–45, 2024. 1
- [5] Z. Chen, J. Wu, W. Wang, W. Su, G. Chen, S. Xing, M. Zhong, Q. Zhang, X. Zhu, L. Lu, B. Li, P. Luo, T. Lu, Y. Qiao, and J. Dai. Internvl: Scaling up vision foundation models and aligning for generic visual-linguistic tasks. In *Proceedings of CVPR*, pages 24185–24198, 2024. 1, 6
- [6] Zhiwei Chen, Xudong Zhang, Chao Liu, Hongyu Zhang, Yuxin Sun, and Yanfeng Zhang. Revisiting slo and goodput metrics in llm serving. [arXiv:2410.14257](https://arxiv.org/abs/2410.14257), 2024. 2
- [7] Cunchen Hu, Heyang Huang, Liangliang Xu, Xusheng Chen, Jiang Xu, Shuang Chen, Hao Feng, Chenxi Wang, Sa Wang,

- Yungang Bao, et al. Inference without interference: Disaggregate llm inference for mixed downstream workloads. [arXiv:2401.11181](#), 2024. 1
- [8] Frank Hutter, Holger H. Hoos, Kevin Leyton-Brown, and Thomas Stützle. Paramils: An automatic algorithm configuration framework. *Journal of Artificial Intelligence Research*, 36:267–306, 2009. 6
- [9] Yibo Jin, Tao Wang, Huimin Lin, Mingyang Song, Peiyang Li, Yipeng Ma, Yicheng Shan, Zhengfan Yuan, Cailong Li, Yajing Sun, et al. P/d-serve: Serving disaggregated large language model at scale. [arXiv:2408.08147](#), 2024. 1
- [10] Woosuk Kwon, Zhuohan Li, Siyuan Zhuang, Ying Sheng, Lianmin Zheng, Cody Hao Yu, Joseph E. Gonzalez, Hao Zhang, and Ion Stoica. Efficient memory management for large language model serving with pagedattention. In *Proceedings of the ACM SIGOPS 29th Symposium on Operating Systems Principles*, 2023. 2, 6
- [11] Haotian Liu, Chunyuan Li, Qingyang Wu, and Yong Jae Lee. Visual instruction tuning. In *Proceedings of NeurIPS*, 2023. 1
- [12] Huan Liu, Yujie Zhang, Xue Yang, Xiaowei Li, Huan Chen, Jure Zhu, and Yu Gong. A survey of resource-efficient llm and multimodal foundation models. [arXiv:2401.08092](#), 2024. 1, 2
- [13] NVIDIA Corporation. Triton Inference Server: An Optimized Cloud and Edge Inferencing Solution. 2
- [14] Pratyush Patel, Esha Choukse, Chaojie Zhang, Aashaka Shah, Íñigo Goiri, Saeed Maleki, and Ricardo Bianchini. Splitwise: Efficient generative llm inference using phase splitting. In *2024 ACM/IEEE 51st Annual International Symposium on Computer Architecture (ISCA)*, pages 118–132, 2024. 1, 2
- [15] Ruoyu Qin, Zheming Li, Weiran He, Mingxing Zhang, Yongwei Wu, Weimin Zheng, and Xinran Xu. Mooncake: A kvcache-centric disaggregated architecture for llm serving. [arXiv:2407.00079](#), 2024. 1
- [16] Foteini Strati, Sara Mcallister, Amar Phanishayee, Jakub Tarnawski, and Ana Klimovic. Déjàvu: Kv-cache streaming for fast, fault-tolerant generative llm serving. In *ICML*, 2024. 2
- [17] The PyTorch Team. PyTorch Serve, 2024. 2
- [18] Thomas Wolf, Lysandre Debut, Victor Sanh, Julien Chaumond, Clement Delangue, Anthony Moi, Pierric Cistac, Tim Rault, Rémi Louf, Morgan Funtowicz, Joe Davison, Sam Shleifer, Patrick von Platen, Clara Ma, Yacine Jernite, Julien Plu, Canwen Xu, Teven Le Scao, Sylvain Gugger, Mariama Drame, Quentin Lhoest, and Alexander M. Rush. Transformers: State-of-the-art natural language processing. In *Proceedings of the 2020 Conference on Empirical Methods in Natural Language Processing: System Demonstrations*, pages 38–45, 2020. 2
- [19] Bingyang Wu, Yinmin Zhong, Zili Zhang, Shengyu Liu, Fangyue Liu, Yuanhang Sun, Gang Huang, Xuanzhe Liu, and Xin Jin. Fast distributed inference serving for large language models. [arXiv:2305.05920v3](#), 2023. 2
- [20] Jiayang Wu, Wensheng Gan, Zefeng Chen, Shicheng Wan, and S Yu Philip. Multimodal large language models: A survey. In *2023 IEEE International Conference on Big Data (BigData)*, pages 2247–2256. IEEE, 2023. 1
- [21] Yuan Yao, Tianyu Yu, Ao Zhang, Chongyi Wang, Junbo Cui, Hongji Zhu, Tianchi Cai, Haoyu Li, Weilin Zhao, Zhihui He, et al. Minicpm-v: A gpt-4v level mllm on your phone. [arXiv:2408.01800](#), 2024. 1, 6, 7
- [22] Gyeong-In Yu, Joo Seong Jeong, Geon-Woo Kim, Soojeong Kim, and Byung-Gon Chun. Orca: A distributed serving system for Transformer-Based generative models. In *16th USENIX Symposium on Operating Systems Design and Implementation (OSDI 22)*, pages 521–538, 2022. 2
- [23] Lianmin Zheng, Liangsheng Yin, Zhiqiang Xie, Chuyue Sun, Jeff Huang, Cody Hao Yu, Shiyi Cao, Christos Kozyrakis, Ion Stoica, Joseph E. Gonzalez, Clark Barrett, and Ying Sheng. Sglang: Efficient execution of structured language model programs. [arXiv:2312.07104](#), 2023. 2
- [24] Yinmin Zhong, Shengyu Liu, Junda Chen, Jianbo Hu, Yibo Zhu, Xuanzhe Liu, Xin Jin, and Hao Zhang. Distserve: Disaggregating prefill and decoding for goodput-optimized large language model serving. In *OSDI*, pages 193–210. USENIX Association, 2024. 1, 2, 6
- [25] Zixuan Zhou, Xuefei Ning, Ke Hong, Tianyu Fu, Jiaming Xu, Shiyao Li, Yuming Lou, Luning Wang, Zhihang Yuan, Xiuhong Li, Shengen Yan, Guohao Dai, Xiao-Ping Zhang, Yuhan Dong, and Yu Wang. A survey on efficient inference for large language models. [arXiv:2404.14294](#), 2024. 2